

Misfit phase $(\text{BiSe})_{1.10}\text{NbSe}_2$ as the origin of superconductivity in niobium-doped bismuth selenide

Machteld E. Kamminga ¹, Maria Batuk², Joke Hadermann ² & Simon J. Clarke ¹✉

Topological superconductivity is of great contemporary interest and has been proposed in doped Bi_2Se_3 , in which electron-donating atoms such as Cu, Sr or Nb have been intercalated into the Bi_2Se_3 structure. For $\text{Nb}_x\text{Bi}_2\text{Se}_3$, with $T_c \sim 3$ K, it is assumed in the literature that Nb is inserted in the van der Waals gap. However, in this work an alternative origin for the superconductivity in Nb-doped Bi_2Se_3 is established. In contrast to previous reports, it is deduced that Nb intercalation in Bi_2Se_3 does not take place. Instead, the superconducting behaviour in samples of nominal composition $\text{Nb}_x\text{Bi}_2\text{Se}_3$ results from the $(\text{BiSe})_{1.10}\text{NbSe}_2$ misfit phase that is present in the sample as an impurity phase for small x ($0.01 \leq x \leq 0.10$) and as a main phase for large x ($x = 0.50$). The structure of this misfit phase is studied in detail using a combination of X-ray diffraction and transmission electron microscopy techniques.

¹Department of Chemistry, University of Oxford, Inorganic Chemistry Laboratory, South Parks Road, Oxford OX1 3QR, UK. ²Electron Microscopy for Materials Science (EMAT), University of Antwerp, Groenenborgerlaan 171, B-2020 Antwerp, Belgium. ✉email: simon.clarke@chem.ox.ac.uk

Recently there has been significant interest in layered topological insulators such as the chalcogenides Bi_2Se_3 and Bi_2Te_3 ^{1–6}. Topological insulators are phases of matter in which the bulk material is semiconducting, but the surface contains electrons that are chiral, massless and conduct electricity as though they were metals. Of particular interest is topological superconductivity, which features the existence of gapless surface states at the surface of a fully gapped semiconductor. Because of their unique electronic structure, topological superconductors are proposed to have great potential in fault-tolerant topological quantum computing⁷. Layered materials often allow for intercalation and/or deintercalation as a way of tuning the chemistry and physics. It has been shown, for example, that intercalation of copper into Bi_2Se_3 is possible and gives rise to superconductivity up to 3.8 K^{8,9}. Moreover, superconductivity (with $T_c \sim 5.5$ K) was observed when Bi_2Te_3 was reacted with Pd to form $\text{Pd}_x\text{Bi}_2\text{Te}_3$ with $x = 0.15, 0.3, 0.5$ and 1⁹. Other reported superconducting intercalates are described by the chemical formulae $\text{Sr}_x\text{Bi}_2\text{Se}_3$ ($T_c \sim 2.5$ K⁷, $T_c \sim 2.9$ K¹⁰) and $\text{Nb}_x\text{Bi}_2\text{Se}_3$ ($T_c \sim 3$ K^{11–13}), where x generally ranges between 0.05 and 0.25. Note that these $\text{M}_x\text{Bi}_2\text{Se}_3$ ($M = \text{Cu}, \text{Sr}, \text{Nb}$) phases are synthesised at elevated temperatures from a stoichiometric ratio of the elements M, Bi and Se. This is in contrast to the work by Koski et al., where zerovalent metals are intercalated, at around ambient temperature, into Bi_2Se_3 post synthesis, and complex superstructures as a result of the ordering of the intercalated atoms are obtained¹⁴.

The chemical nature of these superconducting phases and the location of the intercalated metals in the chalcogenide structure is not trivial. For $\text{Cu}_x\text{Bi}_2\text{Se}_3$, synthesised at high temperatures from the elements, Cu is reckoned to be inserted in the van der Waals gap between the Bi_2Se_3 quintuple layers^{8,15}, as confirmed by the significant increase in the c -axis lattice parameter from $c = 28.666$ (1) Å for Bi_2Se_3 to $c = 28.736$ (1) Å for $\text{Cu}_{0.12}\text{Bi}_2\text{Se}_3$ ⁸. A comparable expansion of the unit cell volume is observed by Koski et al.¹⁴ using intercalation techniques. On the other hand, for phases described with the formula $\text{Sr}_x\text{Bi}_2\text{Se}_3$, there is no clear consensus on the structure. Competing studies state or assume variously that Sr is inserted in the van der Waals gap¹⁰ or within the quintuple layers themselves¹⁶. For $\text{Nb}_x\text{Bi}_2\text{Se}_3$, it was concluded from apparent small shifts in peak positions in powder diffraction measurements that the c -axis length expanded slightly leading to the assumption that Nb is inserted in the van der Waals gap of Bi_2Se_3 and the compound has a similar structure to $\text{Cu}_x\text{Bi}_2\text{Se}_3$ ^{12,17}. The minimal change in lattice parameters implies a highly distorted coordination environment for Nb¹⁷. Several papers on $\text{Nb}_x\text{Bi}_2\text{Se}_3$ describe a range of detailed examinations of the superconducting properties, but in many of these works presented on $\text{Nb}_x\text{Bi}_2\text{Se}_3$ samples, the extent of the bulk characterisation of the samples is limited. Kobayashi et al.¹¹ synthesised $\text{Nb}_x\text{Bi}_2\text{Se}_3$ with varying x and did examine the samples using bulk powder diffraction measurements. These showed, in addition to a phase with the Bi_2Se_3 structure, an impurity phase to which they assigned the formula BiNbSe_3 ¹⁸ and a second impurity, BiSe. These impurities increased in fraction with increasing x and indeed they showed that the phase fraction of the proposed $\text{Nb}_x\text{Bi}_2\text{Se}_3$ phase with the Bi_2Se_3 structure reaches zero (within the uncertainty) at $x = 0.50$. Work by Wang et al.¹⁹ and recent work by Cho et al.²⁰ also show that $\text{Nb}_x\text{Bi}_2\text{Se}_3$ samples are multiphase in the bulk. Nevertheless, all these reports assign the superconductivity evident in these samples to a Nb-doped Bi_2Se_3 -type phase.

Here we show evidence for an alternative explanation for the observed superconductivity in Nb-doped Bi_2Se_3 samples of overall composition $\text{Nb}_x\text{Bi}_2\text{Se}_3$. We show that conventional high-temperature synthesis of samples with the composition $\text{Nb}_x\text{Bi}_2\text{Se}_3$ ($0 \leq x \leq 0.50$) results in a mixture of three phases: Bi_2Se_3 , BiSe and

the layered misfit compound $(\text{BiSe})_{1.10}\text{NbSe}_2$. This so-called misfit compound is a layered composite (i.e. an intergrowth) compound made up of two (or more) interpenetrating sublattices of different chemical composition²¹. For $(\text{BiSe})_{1.10}\text{NbSe}_2$, the two sublattices of composition BiSe and NbSe_2 occur with a ratio of 1.10:1 and have different intralayer lattice constants, which do not match, hence the term *misfit*, and the corresponding misfit ratio is evident in the formula. In this paper and particularly in the supporting information we describe the structure in detail and show how $(\text{BiSe})_{1.10}\text{NbSe}_2$ compares with related misfit layered chalcogenides. This misfit phase corresponds to the peaks previously assigned to the BiNbSe_3 impurity¹⁸ (which is of fairly similar composition) by Kobayashi et al.¹¹ and by Cho et al.²⁰ We observe that the amount of the phase present with the Bi_2Se_3 structure (assumed to be the superconducting phase $\text{Nb}_x\text{Bi}_2\text{Se}_3$ in the literature^{11,12,17,19,20,22–26}, including very recent literature^{19,20,24,25}) in the samples decreases with increasing Nb content in the synthesis mixture and completely vanishes for $x = 0.50$ while the superconducting volume fraction of the sample is directly proportional to the Nb content of the sample. In addition we do not observe, with synchrotron resolution, a measurable c -axis expansion of the Bi_2Se_3 -structure phase upon Nb doping, suggesting that it is pure and undoped Bi_2Se_3 . Moreover, our energy-dispersive X-ray spectroscopy (EDX) measurements reveal no crystallites with elemental composition $\text{Nb}_x\text{Bi}_2\text{Se}_3$. Therefore, in contrast to previous reports, we deduce that Nb doping in Bi_2Se_3 does not take place and the superconducting behaviour in samples of composition $\text{Nb}_x\text{Bi}_2\text{Se}_3$ is actually caused by the misfit phase $(\text{BiSe})_{1.10}\text{NbSe}_2$ that is present in the sample as an impurity phase for small x and as a main phase for large x .

Results and discussion

Composition dependence of structures and superconducting properties. Figure 1a shows the synchrotron powder diffraction pattern of a sample of composition $\text{Nb}_{0.20}\text{Bi}_2\text{Se}_3$, which is a typical diffraction pattern of these $\text{Nb}_x\text{Bi}_2\text{Se}_3$ samples. It is clear that this $\text{Nb}_{0.20}\text{Bi}_2\text{Se}_3$ sample consists of three phases as indicated by the fit and coloured markers: a phase with the Bi_2Se_3 structure, the misfit phase $(\text{BiSe})_{1.10}\text{NbSe}_2$, and BiSe. The fit for the Bi_2Se_3 structure phase resulted in lattice parameters of $a = 4.1390$ (8) Å and $c = 28.6298$ (10) Å which are equal within one estimated standard deviation in the refinement to those of pure Bi_2Se_3 ($a = 4.1393$ (11) Å and $c = 28.6304$ (9) Å) which we measured with synchrotron radiation under the same conditions, from which we conclude that there is no evidence for Nb intercalation. Figure 1c–e shows representative scanning electron microscopy (SEM) energy-dispersive X-ray spectroscopy (EDX) maps of the sample. Figure 1b shows crystallites with different elemental composition corresponding to either $(\text{BiSe})_{1.10}\text{NbSe}_2$ with a Nb:Bi ratio close to 1:1 or Nb-free Bi and Se phases, i.e. no crystallites with a composition close to $\text{Nb}_x\text{Bi}_2\text{Se}_3$ are observed for this sample with $x = 0.2$ in the reaction mixture. The chemical composition of the misfit phase was determined by SEM-EDX as Bi/Se/Nb: 22(1)/59(1)/19(1) (Fig. 1) and additionally by scanning transmission electron microscopy (STEM) EDX measurements as Bi/Se/Nb: 21.4(2)/60.5(8)/18.1(7) (Supplementary Fig. S10), which are in agreement within the experimental uncertainty. Moreover, Nb is only found in combination with Bi and Se in a ratio corresponding to $(\text{BiSe})_{1.10}\text{NbSe}_2$, no other Nb-containing phase such as NbSe_2 is observed.

In Fig. 2a, we show the superconducting properties of samples made with compositions $\text{Nb}_x\text{Bi}_2\text{Se}_3$. The critical temperature T_c of roughly 3.2 K is in agreement with previous reports of superconductivity in samples of these nominal compositions^{11–13}. Moreover, the superconducting volume fraction is directly

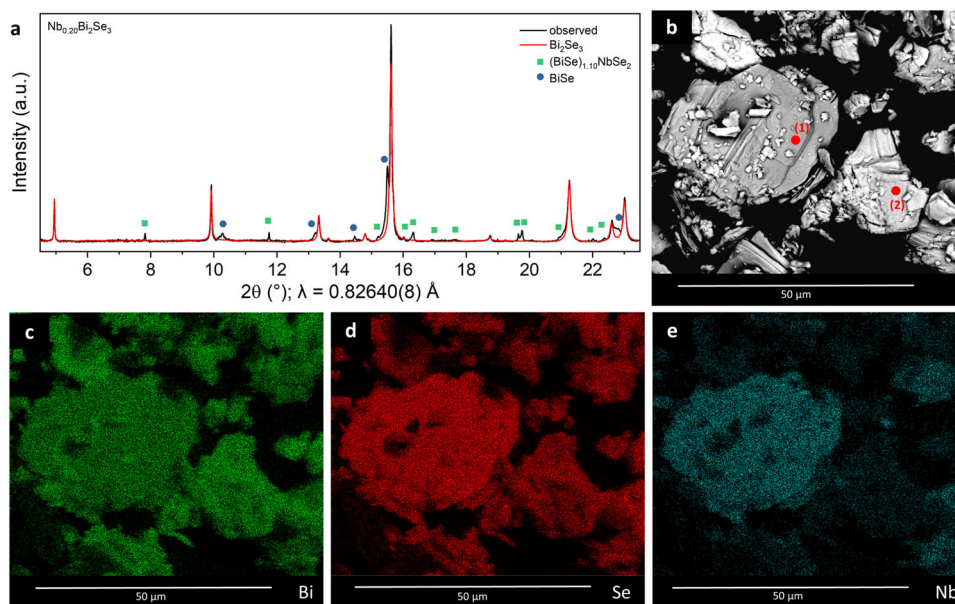


Fig. 1 Diffraction and electron microscopy data of $\text{Nb}_{0.20}\text{Bi}_2\text{Se}_3$. **a** Synchrotron X-ray diffraction pattern of $\text{Nb}_{0.20}\text{Bi}_2\text{Se}_3$ fitted with Bi_2Se_3 . Green squares and blue dots indicate impurity phases of the misfit phase $(\text{BiSe})_{1.10}\text{NbSe}_2$ and BiSe , respectively. **b** Electron Backscatter Diffraction (EBSD) image of the same sample showing crystallites with different average Z value. Point (1) has an elemental ratio of $\sim 1\text{Nb}:-1.1\text{Bi}:-3\text{Se}$, which closely resembles $(\text{BiSe})_{1.10}\text{NbSe}_2$ ³⁵, whereas point (2) has an elemental ratio of $\sim 2\text{Bi}:-3.4\text{Se}$ with no Nb present. **c-e** EDX maps corresponding to **(b)** showing the presence of Bi, Se and Nb in the crystallites.

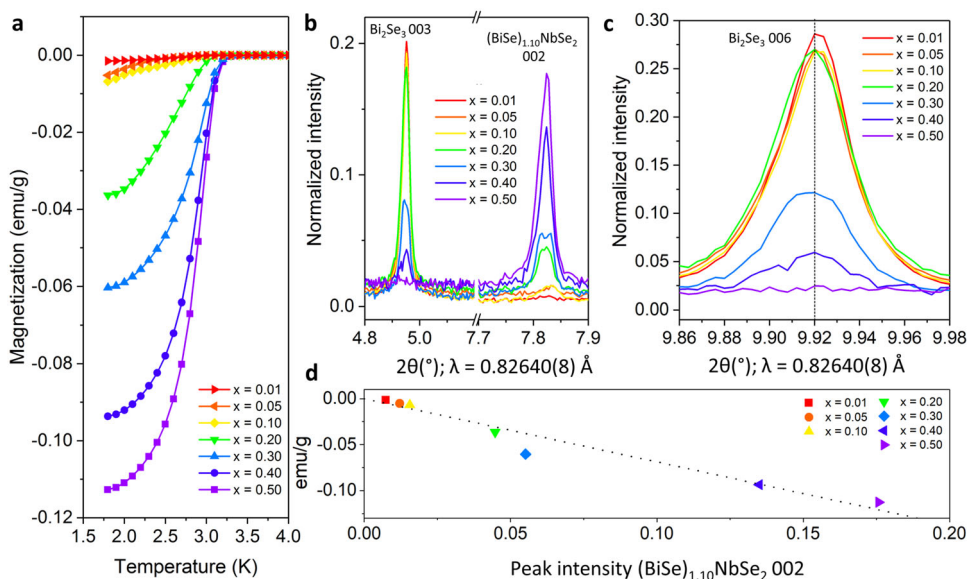


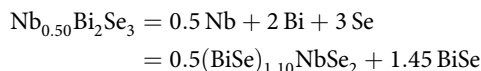
Fig. 2 Relation between magnetometry and diffraction in $\text{Nb}_x\text{Bi}_2\text{Se}_3$. **a** Magnetometry results (ZFC: zero-field cooled) for $\text{Nb}_x\text{Bi}_2\text{Se}_3$ with varying Nb content. A full plot also containing the FC (field cooled) data is shown in Supplementary Fig. S1. **b** Selected peaks of the corresponding diffraction patterns indicating the relative intensities of the Bi_2Se_3 and $(\text{BiSe})_{1.10}\text{NbSe}_2$ phases for varying Nb content. **c** Normalized intensity of the Bi_2Se_3 006 peak with varying x . **d** Relation between the peak intensity of the 002 peak of $(\text{BiSe})_{1.10}\text{NbSe}_2$ (from **b**) and magnetization at 1.8 K (from **a**) with varying Nb content of the samples.

proportional to x . We state the susceptibility per gram of material due to the fact that the $\text{Nb}_x\text{Bi}_2\text{Se}_3$ sample is a mixture of three phases and the ratios of these phases differ for different x . Figure 2b shows the first two characteristic peaks of the diffraction pattern: the 003 peak of the Bi_2Se_3 -structure phase and the 002 peak of $(\text{BiSe})_{1.10}\text{NbSe}_2$. The intensity of the Bi_2Se_3 -structure 003 peak is reduced upon increasing x and for $x = 0.50$ there is no evidence for a Bi_2Se_3 -structure phase present in the sample. Moreover, as quantified above, we do not observe any

evidence, with synchrotron resolution, for a measurable peak shift and hence a c -axis expansion within one estimated standard deviation of this Bi_2Se_3 -structure phase present in the samples upon Nb doping (see Fig. 2c) suggesting that it is undoped Bi_2Se_3 . This is in contrast to the variations stated in literature reports. However, these reports either do not refine the lattice parameters from the whole pattern¹¹, or do not present any uncertainties on the refined values¹⁹, or do not make a comparison using the same measurement conditions with a pure Bi_2Se_3 phase²⁰. Wang et al.¹⁹

report a slight expansion in c on Nb doping, but do not report the estimated standard deviation and Cho et al.²⁰ report a c lattice parameter of 28.4633(7) Å, which is much smaller than what we and Wang et al.¹⁹ find for pure Bi₂Se₃. Our previous work on Li_{1-x}Fe_{1+x}As samples showed that trends in lattice parameters arising from very small compositional changes could only be monitored by synchrotron radiation²⁷. Our observation of no c -axis expansion within one estimated standard deviation with synchrotron resolution is strong evidence that no intercalation of Nb into Bi₂Se₃ took place. This argument, in combination with the fact that the superconducting volume fraction increases with x while the amount of the Bi₂Se₃-structure phase decreases with x , proves that the superconductivity does not arise from a Bi₂Se₃-structure phase. Thus, the superconductivity does not arise from the assumed intercalate Nb_xBi₂Se₃ phase with Nb intercalated between or within Bi₂Se₃ slabs or substituted for one of the other elements. Particularly compelling is that the superconducting volume fraction is highest when there is no Bi₂Se₃-structure phase present within the detection limits of the synchrotron powder diffraction experiment. In addition, the intensity of the 002 peak of (BiSe)_{1.10}NbSe₂ is directly proportional to the superconducting volume fraction (Fig. 2d). For small x , (BiSe)_{1.10}NbSe₂ can be considered a small superconducting impurity and for larger x , the (BiSe)_{1.10}NbSe₂ phase dominates. Note that Fig. 2a shows that there appears to be a slight variation in T_c (between 3.0 and 3.2 K) among samples prepared under similar conditions with various Nb contents. As will be highlighted below, (BiSe)_{1.10}NbSe₂ is subject to small variations in T_c depending on synthesis technique, and can contain various stacking faults.

As shown in Fig. 1, BiSe is also present in Nb_xBi₂Se₃ samples in addition to Bi₂Se₃ and (BiSe)_{1.10}NbSe₂. As can be seen in Fig. 2b, when x reaches 0.5, Nb_{0.50}Bi₂Se₃ contains no phase with the structure of Bi₂Se₃ and therefore solely consists of the misfit phase (BiSe)_{1.10}NbSe₂ and BiSe according to the equation:



Our investigation of the relationship between the superconducting volume fraction and the ratio of (BiSe)_{1.10}NbSe₂ and BiSe in Nb_{0.50}Bi₂Se₃ reveals that the superconducting volume fraction increases with the (BiSe)_{1.10}NbSe₂/BiSe ratio, confirming that the misfit phase is responsible for the superconducting properties in samples of composition Nb_xBi₂Se₃ and BiSe is not. A full description of this investigation is given in Supplementary Section 1 and Supplementary Fig. S5.

Figure 3 shows the magnetometry data for the sample of composition Nb_{0.50}Bi₂Se₃ in comparison with the superconducting properties of its two constituents, i.e. BiSe and the misfit phase (BiSe)_{1.10}NbSe₂ synthesised in pure form (see ‘Methods’ section). The pure BiSe sample is not superconducting while the pure misfit phase is superconducting with a similar T_c as that found for the mixed-phase sample of composition Nb_{0.50}Bi₂Se₃ as shown in Fig. 2. Note that bulk 2H-NbSe₂ is a well-studied superconductor with a $T_c \sim 7 \text{ K}$ ^{28–31}. Monolayer NbSe₂ has a $T_c \sim 3 \text{ K}$ ³², which is similar to (BiSe)_{1.10}NbSe₂. This is consistent with the misfit phase being effectively constructed of single layers of NbSe₂ separated by the BiSe layers. Since the scanning electron microscopy (SEM) data of Supplementary Fig. S4 reveal that this Nb_{0.50}Bi₂Se₃ sample contains no crystallites with the Nb_xBi₂Se₃ composition and solely consists of BiSe and (BiSe)_{1.10}NbSe₂, as confirmed by the synchrotron X-ray diffraction (XRD) data from Fig. 2, this data directly proves that the superconductivity in Nb_{0.50}Bi₂Se₃ and therefore in all our Nb_xBi₂Se₃ samples is caused by the superconducting (BiSe)_{1.10}NbSe₂ misfit compound.

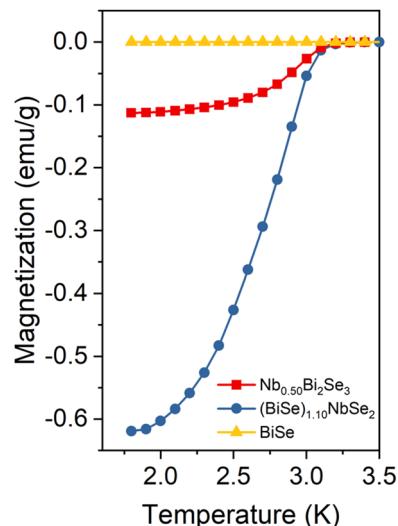


Fig. 3 Magnetometry results (ZFC) for Nb_{0.50}Bi₂Se₃. Nb_{0.50}Bi₂Se₃ (a mixture of solely BiSe and (BiSe)_{1.10}NbSe₂, as shown in Fig. 2 and Supplementary Fig. S4), BiSe and the pure misfit phase (BiSe)_{1.10}NbSe₂. A full plot also containing the FC data is shown in Supplementary Fig. S2.

Several papers report the presence of BiNbSe₃ impurities, but do not regard these impurities as relevant for the reported physical properties^{11,19,20}. Wang et al.¹⁹ attempted to make this impurity as a pure phase, but no structure or physical properties were given. Our diffraction and electron microscopy measurements, as discussed below, show that the peaks assigned to the BiNbSe₃ phase¹⁸ could actually be assigned to the superconducting (BiSe)_{1.10}NbSe₂ misfit phase. Thus, to the best of our knowledge, no single phase of alleged Nb_xBi₂Se₃ nor direct proof of Nb intercalation into Bi₂Se₃ by means of single-crystal XRD, electron diffraction or electron microscopy imaging techniques is reported to date.

A large portion of the published work on the interesting physical properties reported for Nb_xBi₂Se₃ is performed on single crystals^{12,13,20,22,33,34}, that are provided by a single research group who described their synthesis method in ref. 17. The most recent of these papers by Cho et al.²⁰, performed bulk analysis on a sample of nominal composition Nb_{0.25}Bi₂Se₃ in response to the published referee report. According to the published powder diffraction pattern, that analysis showed that the sample used was a similar multiphase mixture to those which we report here, and there is also consistency with the work of Kobayashi et al.¹¹. Thus, all the published works which show bulk analysis of Nb_xBi₂Se₃ samples show multiphase behaviour, and the published works on single crystals mentioned above have studied single crystals that were selected from these multiphase batches.

As shown in Supplementary Fig. S3, we found a small variation in T_c of (BiSe)_{1.10}NbSe₂ depending on the synthesis technique. Herein, we show the magnetometry data of naturally cooled (i.e. at the rate of the furnace when switched off) and ice/water quenched pure misfit samples as obtained by the vapour transport method³⁵. The naturally cooled sample has a $T_c \sim 2.3 \text{ K}$ which is in good agreement with previous reports on the superconducting properties of the misfit phase³⁶. The ice/water quenched sample has a significantly higher T_c that is comparable to the ice/water quenched samples of Nb_xBi₂Se₃ shown in Fig. 2a. We do not observe any notable difference in the X-ray patterns between the samples. The (BiSe)_{1.10}NbSe₂ data in Fig. 3 is obtained by annealing the ice/water quenched sample at 640 °C for a couple of days. We hypothesise that the small changes in properties are caused by either minuscule compositional changes

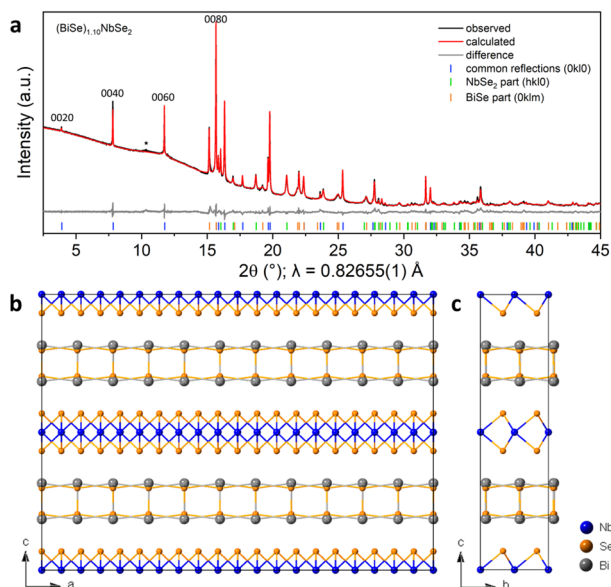


Fig. 4 Diffraction pattern and crystal structure of $(\text{BiSe})_{1.10}\text{NbSe}_2$. **a** Rietveld fit to synchrotron data of $(\text{BiSe})_{1.10}\text{NbSe}_2$. All peaks can be indexed with solely the main reflections of both sublattices. A few 00/0 peaks are indicated for clarity. The star symbol represents a tiny amount of BiSe impurity. **b, c** Average crystal structure of $(\text{BiSe})_{1.10}\text{NbSe}_2$. The average structure drawn with anisotropic displacement ellipsoids is shown in Supplementary Fig. S7.

(e.g. Se deficiencies) or potentially different NbSe_2 stacking faults (see below) that can be present in the $(\text{BiSe})_{1.10}\text{NbSe}_2$ compound. This study will be part of future investigations. Similar variation in the T_c of halide-flux-grown crystals with compositions close to NbBiSe_3 has recently been reported³⁷.

Structural analysis of $(\text{BiSe})_{1.10}\text{NbSe}_2$. $(\text{BiSe})_{1.10}\text{NbSe}_2$ has been synthesised and studied previously^{35,36}, but complete structure solution by single-crystal X-ray diffraction was hampered, apparently by disorder in the BiSe sublattice along the stacking direction. To probe the structure of the misfit phase $(\text{BiSe})_{1.10}\text{NbSe}_2$ in more detail we synthesized it phase pure from the elements using a vapour transport synthesis method³⁵. Powder diffraction data (Fig. 4a) are in agreement with those of Zhou et al.³⁵. Single-crystal X-ray diffraction measurements performed on the I19 beamline at Diamond Light Source (UK) show severely streaked reflections parallel to c (Supplementary Fig. S6), confirming a type of disorder intrinsic to this phase and restricting the amount of structural information available from single-crystal X-ray diffraction. Refinement of composite structures from powder diffraction data^{38–40}, gives less detailed models than those obtained from single-crystal X-ray diffraction³⁹ as there is no reliable method to determine a modulation vector from powder data³⁸. Therefore, as the starting point for refining the crystal structure from synchrotron powder X-ray data, we performed transmission electron microscopy and combined its results with the previously published model for $(\text{BiSe})_{1.09}\text{TaSe}_2$ ^{35,41}, which is very similar to $(\text{BiSe})_{1.10}\text{NbSe}_2$ ³⁵. A detailed description of the modelling of the average crystal structure of $(\text{BiSe})_{1.10}\text{NbSe}_2$ (summarised in Fig. 4b, c) from synchrotron powder data and electron diffraction data is given in Supplementary Section 2 and Supplementary Figs. S8 and S9. In this description, the crystal consists of two separate translationally symmetric subsystems. Due to their mutual interaction, the subsystems will in reality be modulated⁴².

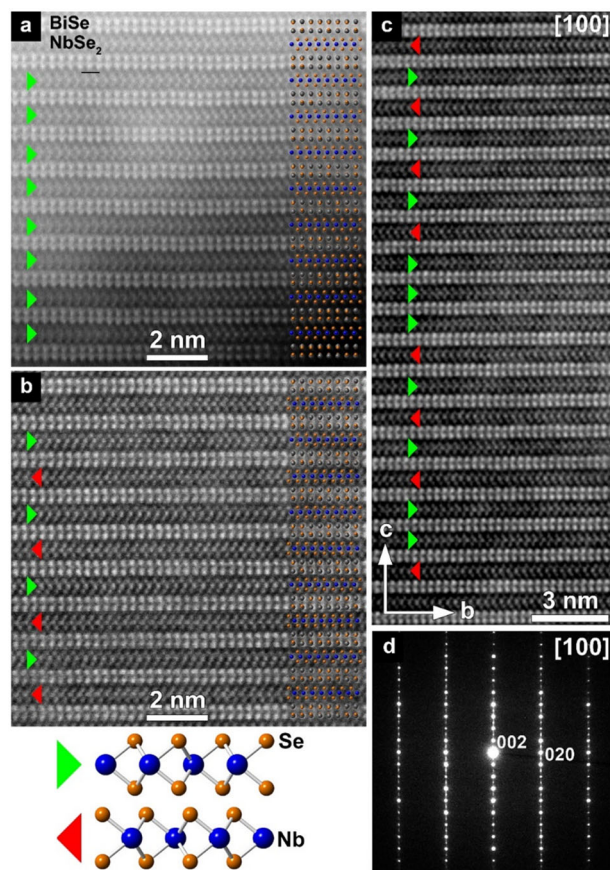


Fig. 5 [100] HAADF-STEM images and electron diffraction pattern of $(\text{BiSe})_{1.10}\text{NbSe}_2$. The HAADF-STEM images clearly show a layered structure with alternating BiSe (appear brighter due to $Z_{\text{Bi}} = 83$) and NbSe_2 (appear weaker due to $Z_{\text{Nb}} = 41$) blocks. Structure overlay with **a** demonstrating all identical NbSe_2 layers and **b** mirrored NbSe_2 layers the c -direction. **c** HAADF-STEM image from a larger area showing a random distribution of the NbSe_2 layers. **d** Corresponding electron diffraction pattern showing elongated reflections $Ok_l: l = 2n + 1$ due to the stacking faults.

In order to gain more insight into the local structure of $(\text{BiSe})_{1.10}\text{NbSe}_2$ and how it differs from that of the Ta analogue, and to explain the origin of the streaking in the single-crystal diffraction patterns, we performed high-angle annular dark-field (HAADF) scanning transmission electron microscopy (STEM) imaging. Figure 5a, b shows representative HAADF-STEM images acquired along the [100] direction. They clearly show a layered structure with alternating BiSe and NbSe_2 blocks. The thickness of the blocks and their [100] orientation were constant in the whole area of investigation. The synthesis technique used here leads to a more uniform structure than the layer-by-layer vapour deposition employed by Mitchson et al.^{43,44}. The structure of $(\text{BiSe})_{1.10}\text{NbSe}_2$, refined (Fig. 4a) using the $(\text{BiSe})_{1.09}\text{TaSe}_2$ ^{35,41} model as a starting point, is overlaid on the images. The image in Fig. 5a perfectly matches the refined structure from Fig. 4b, c and all NbSe_2 layers have the same orientation (as indicated by the green triangles which indicate the orientation of the NbSe_6 triangular prisms). However, in some regions of the crystals, some of the NbSe_2 layers have two different orientations, and the two orientations are related by a reflection in the ac plane. The second orientation is represented by the red triangles. The presence of the two orientations can be seen from the shifts of Nb and Se atomic columns in Fig. 5b and as depicted in the figure legend. The two types of NbSe_2 layers with opposing orientations of the NbSe_6

triangular prisms can perfectly alternate along the stacking direction (Fig. 5b) or occur in a random manner (Fig. 5c), obtaining the character of stacking faults. The corresponding electron diffraction pattern acquired from a large area is shown in Fig. 5d. It can be indexed with the cell parameters $b \approx 6.0 \text{ \AA}$, $c \approx 24.0 \text{ \AA}$, in agreement with the refinement parameters in Supplementary Tables S1 and S2, but shows elongated reflections $0kl$ when l is odd, which is in agreement with the occurrence of these stacking faults and explains the streaked reflections observed for single-crystal X-ray diffraction in Supplementary Fig. S6 and as described in reference 35 which accounts for the difficulty in refining the structure from single-crystal data, and is a difference between $(\text{BiSe})_{1.10}\text{NbSe}_2$ and the Ta analogue. Further explanation of how these stacking faults observed by STEM relate to the powder pattern as shown in Fig. 4a is given in the Supplementary Section 3, Supplementary Figs. S10–S12 and Supplementary Table S3.

Concluding remarks. In conclusion, there are several reports in the literature of derivatives of the important narrow band gap semiconductor Bi_2Se_3 which show superconductivity. A notable contemporary example is the case of samples with the proposed formula $\text{Nb}_x\text{Bi}_2\text{Se}_3$. In this work, we show that there is no evidence for the chemically surprising formation of phases in which Nb is intercalated between the Bi_2Se_3 quintuple layer slabs or otherwise inserted or substituted into the Bi_2Se_3 structure. We conclude from analysis of high-resolution powder diffraction data, transmission electron microscopy and magnetometry measurements on samples of overall composition $\text{Nb}_x\text{Bi}_2\text{Se}_3$ ($0 \leq x \leq 0.50$) that pure $\text{Nb}_x\text{Bi}_2\text{Se}_3$ phases with the Bi_2Se_3 structure are not attainable using high-temperature synthetic methods, and that the superconductivity in these compositions arises from the misfit phase $(\text{BiSe})_{1.10}\text{NbSe}_2$ which is a composite of NbSe_2 and BiSe slabs. This evident inhomogeneity of samples of nominal composition $\text{Nb}_x\text{Bi}_2\text{Se}_3$ might also explain why in one report it was noted that not all of the samples were of high enough quality to show a large superconducting volume fraction³³. Furthermore, the upper critical field data are reportedly dominated by two-fold symmetry, in contradiction to the three-fold symmetry of the Bi_2Se_3 structure which led to the proposal of a nematic state²². We suggest that it should be checked whether the orthorhombic two-fold symmetry of the superconducting misfit phase $(\text{BiSe})_{1.10}\text{NbSe}_2$ can account for the upper critical field response.

Methods

Synthesis. Polycrystalline samples of composition $\text{Nb}_x\text{Bi}_2\text{Se}_3$ ($x = 0.01, 0.05, 0.10, 0.20, 0.30, 0.40, 0.50$) were synthesized by mixing together stoichiometric ratios of high-purity Bi pieces (Sigma-Aldrich; 99.999%), Se powder (Alfa Aesar; 99.999%) and Nb powder (Alfa Aesar; 99.99%), and heating them in an evacuated sealed silica tube to $850 \text{ }^\circ\text{C}$ at $30 \text{ }^\circ\text{C h}^{-1}$. After holding the temperature for 72 h, the powders were cooled slowly to $610 \text{ }^\circ\text{C}$ at $3 \text{ }^\circ\text{C h}^{-1}$ and finally quenched into ice/water after which the obtained products were ground into a fine powder. This procedure is closely related to a previously reported procedure for the synthesis of $\text{Sr}_x\text{Bi}_2\text{Se}_3$ ⁷, and was chosen as it was very similar to various reports on the synthesis of $\text{Nb}_x\text{Bi}_2\text{Se}_3$ ^{11,25}, in order to compare the results. The very slow cooling between 850 and $610 \text{ }^\circ\text{C}$ was performed in order to allow crystals to grow from the melt^{11,17,19,25}. Ice/water quenching was performed as this was done in the previous reports^{11,19,25} with which we sought comparison, and it was found to be crucial for obtaining superconductivity in $\text{Sr}_x\text{Bi}_2\text{Se}_3$ ¹⁶. To verify the need for ice/water quenching, we synthesised single crystals of $(\text{BiSe})_{1.10}\text{NbSe}_2$ by a vapour transport method with and without ice/water quenching as detailed below.

Polycrystalline BiSe was synthesised by mixing together stoichiometric ratios of the Bi pieces and Se powder described above, following a previously reported synthesis method⁴⁵. The elements were heated in an evacuated sealed silica tube to $850 \text{ }^\circ\text{C}$ at $2 \text{ }^\circ\text{C min}^{-1}$. After holding the temperature for 1 week, the samples were quenched into ice/water, ground into a fine powder and annealed at $550 \text{ }^\circ\text{C}$ in order to increase crystallinity for roughly 2 months followed by quenching in ice/water.

Single crystals of the layered misfit compound $(\text{BiSe})_{1.10}\text{NbSe}_2$ were synthesized through a previously reported vapour transport method³⁵. A stoichiometric ground mixture of the elements described above was placed in one end of an evacuated

sealed silica tube and this end of the tube was placed in a tube furnace at $700 \text{ }^\circ\text{C}$ with the other end maintained at $640 \text{ }^\circ\text{C}$. Around 10 mg of $(\text{NH}_4)_2\text{PbCl}_6$ per 500 mg of the total mass of the precursors was used as a transport agent. $(\text{NH}_4)_2\text{PbCl}_6$ was prepared by a modified synthesis method⁴⁶ from a stoichiometric mixture of PbO_2 and NH_4 in ice-cold HCl . After around 10 days, the tube was ice/water quenched and the crystals were extracted from the cold end of the tube. Small crystals with sizes up to 0.5 mm were obtained. Naturally cooled samples without ice/water quenching (i.e. cooled at the rate of the tube furnace when switched off) were also prepared and the structures and properties of the obtained crystals were compared.

X-ray diffraction. Powder X-ray diffraction (XRD) measurements were performed on both laboratory XRD equipment (Bruker D8 Advance, Cu K α radiation) and on the I11 beamline at the Diamond Light Source (UK). At I11, diffractograms were measured upon exposure of the monochromatic 15.0 keV ($\lambda = 0.82655(1)$ or $0.82640(8) \text{ \AA}$) calibrated using a Si standard) X-ray beam and collected using a Mythen position-sensitive detector. Single-crystal XRD measurements were performed on the I19 beamline at Diamond Light Source (UK). Data analysis was performed with TOPAS-Academic V5⁴⁷ and Jana2006⁴⁸.

Electron microscopy. Scanning electron microscopy (SEM) measurements were performed using a FEI Quantum FEG 650 operating in low vacuum mode with an accelerator voltage of 20 kV and a spot size of 3.5. Electron diffraction patterns were acquired on a Thermo Fisher Tecna transmission electron microscope (TEM) operated at 200 kV . High-angle annular dark-field (HAADF) scanning transmission electron microscopy (STEM) images and energy-dispersive X-ray spectroscopy (EDX) maps were acquired using a Thermo Fisher Titan 80-300 “cubed” microscope operated at 300 kV . Specimens for the TEM study were prepared in two ways: (1) the material was dispersed in ethanol for 1 h using an ultrasonic bath, with regular breaks to allow the water in the bath to cool. Then, a few drops of the suspension were deposited onto a copper TEM grid covered by a holey carbon layer. (2) The cross-section and plane-view lamellae were prepared from individual crystals using focused ion beam (FIB) milling. During the preparation process, Pt and carbon protective layers were deposited on top of the film. The specimens were prepared in air. TEM images obtained for the specimens prepared by the different methods were consistent. For the compositional analysis by STEM-EDX, Bi-M, Nb-L and Se-K lines were used.

Magnetometry measurements. Magnetic susceptibility measurements were conducted using a Quantum Design MPMS3 superconducting quantum interference device (SQUID) magnetometer. Gelatin capsules were used to contain accurately-weighed powder samples of about $20\text{--}30 \text{ mg}$ in mass. Measurements were performed on warming in a d.c. field of 10 Oe in the temperature range $1.8\text{--}10 \text{ K}$ after firstly cooling in zero applied field (ZFC) and then after cooling in the applied field of 10 Oe (FC).

Data availability

The data that support the findings of this study are available from the corresponding author upon reasonable request.

Received: 18 June 2020; Accepted: 14 October 2020;

Published online: 10 November 2020

References

- He, M., Sun, H. & He, Q. L. Topological insulator: spintronics and quantum computations. *Front. Phys.* **14**, 43401 (2019).
- Liu, P., Williams, J. R. & Cha, J. J. Topological nanomaterials. *Nat. Rev. Mater.* **4**, 479–496 (2019).
- Tang, F., Po, H. C., Vishwanath, A. & Wan, X. Comprehensive search for topological materials using symmetry indicators. *Nature* **566**, 486–489 (2019).
- Xue, H. et al. Realization of an acoustic third-order topological insulator. *Phys. Rev. Lett.* **122**, 244301 (2019).
- Noesges, B. A. et al. Chemical migration and dipole formation at van der Waals interfaces between magnetic transition metal chalcogenides and topological insulators. *Phys. Rev. Mater.* **4**, 054001 (2020).
- Liu, C. W., Wang, Z., Qiu, R. L. J. & Gao, X. P. A. Development of topological insulator and topological crystalline insulator nanostructures. *Nanotechnology* **31**, 192001 (2020).
- Liu, Z. et al. Superconductivity with topological surface state in $\text{Sr}_x\text{Bi}_2\text{Se}_3$. *J. Am. Chem. Soc.* **137**, 10512–10515 (2015).
- Hor, Y. S. et al. Superconductivity in $\text{Cu}_x\text{Bi}_2\text{Se}_3$ and its implications for pairing in the undoped topological insulator. *Phys. Rev. Lett.* **104**, 057001 (2010).
- Hor, Y. S., Checkelsky, J. G., Qu, D., Ong, N. P. & Cava, R. J. Superconductivity and non-metallicity induced by doping the topological insulators Bi_2Se_3 and Bi_2Te_3 . *J. Phys. Chem. Solids* **72**, 572–576 (2011).

10. Shruti, Maurya, Neh, V. K., Srivastava, P. & Patnaik, S. Superconductivity by Sr intercalation in the layered topological insulator Bi_2Se_3 . *Phys. Rev. B* **92**, 020506 (2015).
11. Kobayashi, K., Ueno, T., Fujiwara, H., Yokoya, T. & Akimitsu, J. Unusual upper critical field behavior in Nb-doped bismuth selenides. *Phys. Rev. B* **95**, 180503 (2017).
12. Asaba, T. et al. Rotational symmetry breaking in a trigonal superconductor Nb-doped Bi_2Se_3 . *Phys. Rev. X* **7**, 011009 (2017).
13. Smylie, M. P. et al. Robust odd-parity superconductivity in the doped topological insulator $\text{Nb}_x\text{Bi}_2\text{Se}_3$. *Phys. Rev. B* **96**, 115145 (2017).
14. Koski, K. J. et al. Chemical intercalation of zerovalent metals into 2D layered Bi_2Se_3 nanoribbons. *J. Am. Chem. Soc.* **134**, 13773–13779 (2012).
15. Vasko, A., Tichy, L., Horak, J. & Weissenstein, J. Amphoteric nature of copper impurities in Bi_2Se_3 crystals. *J. Appl. Phys.* **5**, 217–221 (1974).
16. Li, Z. et al. Possible structural origin of superconductivity in Sr-doped Bi_2Se_3 . *Phys. Rev. Mater.* **2**, 014201 (2018).
17. Qiu, Y. et al. Time reversal symmetry breaking superconductivity in topological materials. Preprint at <https://arxiv.org/abs/1512.03519> (2015).
18. Gotoh, Y. et al. Preparation and characterization of BiMX_3 ($M = \text{Ti, V, Nb, Ta}$; $X = \text{S, Se}$), new composite-layered chalcogenides. *Chem. Lett.* **18**, 1559–1562 (1989).
19. Wang, J. et al. Investigate the Nb doping position and its relationship with bulk topological superconductivity in $\text{Nb}_x\text{Bi}_2\text{Se}_3$ by X-ray. *J. Phys. Chem. Solids* **137**, 109208 (2020).
20. Cho, C.-W. et al. Z_2 -vestigial nematic order due to superconducting fluctuations in the doped topological insulators $\text{Nb}_x\text{Bi}_2\text{Se}_3$ and $\text{Cu}_x\text{Bi}_2\text{Se}_3$. *Nat. Commun.* **11**, 3056 (2020).
21. Wiegiers, G. A. et al. Misfit layer compounds $(\text{MS})_n\text{TS}_2$ ($M = \text{Sn, Pb, Bi}$, rare earth elements; $T = \text{Nb, Ta}$; $n = 1.08\text{--}1.19$), a new class of layer compounds. *Solid State Commun.* **70**, 409–413 (1989).
22. Shen, J. et al. Nematic topological superconducting phase in Nb-doped Bi_2Se_3 . *npj Quantum Mater.* **2**, 59 (2017).
23. Yuan, N. F. Q., He, W. Y. & Law, K. T. Superconductivity-induced ferromagnetism and Weyl superconductivity in Nb-doped Bi_2Se_3 . *Phys. Rev. B* **95**, 201109(R) (2017).
24. Yonezawa, S. Nematic superconductivity in doped Bi_2Se_3 topological superconductors. *Condens. Matter.* **4**, 2 (2019).
25. Li, M. et al. Pressure-induced electronic anomaly and multiband superconductivity in the doped topological insulator $\text{Nb}_x\text{Bi}_2\text{Se}_3$. *Phys. Rev. B* **100**, 224521 (2019).
26. Sirohi, A. et al. Low-energy excitations and non-BCS superconductivity in $\text{Nb}_x\text{Bi}_2\text{Se}_3$. *Phys. Rev. B* **98**, 094523 (2018).
27. Pitcher, M. J. et al. Compositional control of the superconducting properties of LiFeAs . *J. Am. Chem. Soc.* **132**, 10467–10476 (2010).
28. Foner, S. & McNiff, E. J. Jr. Upper critical fields of layered superconducting NbSe_2 at low temperatures. *Phys. Lett.* **45A**, 429–430 (1973).
29. de Trey, P., Gygax, S. & Jan, J.-P. Anisotropy of the Ginzburg-Landau parameter K in NbSe_2 . *J. Low Temp. Phys.* **11**, 421–434 (1973).
30. Yokoya, T. et al. Fermi surface sheet-dependent superconductivity in 2H- NbSe_2 . *Science* **294**, 2518–2521 (2001).
31. Rahn, D. J. et al. Gaps and kinks in the electronic structure of the superconductor 2H- NbSe_2 from angle-resolved photoemission at 1 K. *Phys. Rev. B* **85**, 224532 (2012).
32. Xi, X. et al. Ising pairing in superconducting NbSe_2 atomic layers. *Nat. Phys.* **12**, 139–143 (2016).
33. Lawson, B. J. et al. Multiple Fermi surfaces in superconducting Nb-doped Bi_2Se_3 . *Phys. Rev. B* **94**, 041114(R) (2016).
34. Kurter, C. et al. Conductance spectroscopy of exfoliated thin flakes of $\text{Nb}_x\text{Bi}_2\text{Se}_3$. *Nano Lett.* **19**, 38–45 (2019).
35. Zhou, W. Y., Meetsma, A., de Boer, J. L. & Wiegiers, G. A. Characterization and electrical transport properties of the misfit layer compounds $(\text{BiSe})_{1.10}\text{NbSe}_2$ and $(\text{BiSe})_{1.09}\text{TaSe}_2$. *Mat. Res. Bull.* **27**, 563–572 (1992).
36. Nader, A., Briggs, A. & Gotoh, Y. Superconductivity in the misfit layer compounds $(\text{BiSe})_{1.10}(\text{NbSe}_2)$ and $(\text{BiS})_{1.11}(\text{NbS}_2)$. *Solid State Commun.* **101**, 149–153 (1997).
37. Nagao, M. et al. Growth and anisotropy evaluation of NbBiCh_3 ($\text{Ch} = \text{S, Se}$) misfit-layered superconducting single crystals. *Solid State Commun.* **321**, 114051 (2020).
38. Mironov, A. V., Abakumov, A. M. & Antipov, E. V. Powder diffraction of modulated and composite structures. *Rigaku J.* **19&20**, 23–35 (2003).
39. van Smaalen, S., Dinnebier, R., Sofin, M. & Jansen, M. Structures of incommensurate and commensurate composite crystals Na_xCuO_2 ($x = 1.58, 1.6, 1.62$). *Acta Cryst.* **B63**, 17–25 (2007).
40. Akselrud, L., Cardoso Gil, R., Wagner-Reetz, M. & Grin, Y. Disorder in the composite crystal structure of the manganese ‘disilicide’ $\text{MnSi}_{1.73}$ from powder X-ray diffraction data. *Acta Cryst.* **B71**, 707–712 (2015).
41. Petricek, V. et al. The modulated structure of the commensurate misfit-layer compound $(\text{BiSe})_{1.09}\text{TaSe}_2$. *Acta Cryst.* **B49**, 258–266 (1993).
42. van Smaalen, S. Symmetry of composite crystals. *Phys. Rev. B* **43**, 11330–11341 (1991).
43. Mitchson, G., Falmbigl, M., Ditto, J. & Johnson, D. C. Antiphase boundaries in the turbostratically disordered misfit compound $(\text{BiSe})_{1+8}\text{NbSe}_2$. *Inorg. Chem.* **54**, 10309–10315 (2015).
44. Mitchson, G. et al. Structural changes in 2D BiSe bilayers as n increases in $(\text{BiSe})_{1+8}(\text{NbSe}_2)_n$ ($n = 1\text{--}4$) heterostructures. *ACS Nano* **10**, 9489–9499 (2016).
45. Gaudin, E., Jobic, S., Evain, M., Brec, R. & Rouxel, J. Charge balance in some Bi_xSe_y phases through atomic structure determination and band structure calculations. *Mat. Res. Bull.* **30**, 549–561 (1995).
46. Engel, G. Kristallstrukturen einiger hexachlorokomplexsalze. *Z. Krist. Cryst. Mater.* **90**, 341–373 (1935).
47. Coelho, A. A. computer programs TOPAS and TOPAS-Academic: an optimization program integrating computer algebra and crystallographic objects written in C++. *J. Appl. Cryst.* **51**, 210–218 (2018).
48. Petricek, V., Dusek, M. & Palatinus, L. Crystallographic computing system JANA2006: general features. *Z. Krist. Cryst. Mater.* **229**, 345–352 (2014).

Acknowledgements

M.E.K. was supported by the Netherlands Organisation for Scientific Research (NWO, grant code 019.181EN.003). We also acknowledge support from the EPSRC (EP/R042594/1, EP/P018874/1, EP/M020517/1) and the Leverhulme Trust (RPG-2018-377). J.H. acknowledges support from the University of Antwerp through BOF Grant No. 31445. We thank DLS Ltd for beam time (EE18786), Dr Clare Murray for assistance on I11 and Dr Jon Wade from the Department of Earth Sciences, University of Oxford for performing the SEM measurements. We also thank Dr Michal Dušak and Dr Václav Petříček for their advice concerning the use of the Jana2006 software.

Author contributions

M.E.K. and S.J.C. synthesised the compounds, performed the diffraction and magnetometry experiments, and performed the structural refinement. M.B. and J.H. performed the TEM and HAADF-STEM measurements and corresponding analysis. M.E.K. wrote the paper involving all authors.

Competing interests

The authors declare no competing interests.

Additional information

Supplementary information is available for this paper at <https://doi.org/10.1038/s43246-020-00085-z>.

Correspondence and requests for materials should be addressed to S.J.C.

Peer review information Primary handling editor: Aldo Isidori.

Reprints and permission information is available at <http://www.nature.com/reprints>

Publisher's note Springer Nature remains neutral with regard to jurisdictional claims in published maps and institutional affiliations.



Open Access This article is licensed under a Creative Commons Attribution 4.0 International License, which permits use, sharing, adaptation, distribution and reproduction in any medium or format, as long as you give appropriate credit to the original author(s) and the source, provide a link to the Creative Commons license, and indicate if changes were made. The images or other third party material in this article are included in the article's Creative Commons license, unless indicated otherwise in a credit line to the material. If material is not included in the article's Creative Commons license and your intended use is not permitted by statutory regulation or exceeds the permitted use, you will need to obtain permission directly from the copyright holder. To view a copy of this license, visit <http://creativecommons.org/licenses/by/4.0/>.

This article is licensed under a Creative Commons Attribution 4.0 International License, which permits use, sharing, adaptation, distribution and reproduction in any medium or format, as long as you give appropriate credit to the original author(s) and the source, provide a link to the Creative Commons license, and indicate if changes were made. The images or other third party material in this article are included in the article's Creative Commons license, unless indicated otherwise in a credit line to the material. If material is not included in the article's Creative Commons license and your intended use is not permitted by statutory regulation or exceeds the permitted use, you will need to obtain permission directly from the copyright holder. To view a copy of this license, visit <http://creativecommons.org/licenses/by/4.0/>.

© The Author(s) 2020